JOURNAL OF SOLID STATE CHEMISTRY **133,** 279–291 (1997)
ARTICLE NO. SC977456

Borides in Thin Film Technology

Christian Mitterer

Institut für Metallkunde und Werkstoffprüfung, Montanuniversität Leoben, Franz-Josef-Straße 18, A-8700 Leoben, Austria

Received April 14, 1997; accepted April 28, 1997

The borides of transition and rare-earth metals are considered for application as wear- and corrosion-resistant, decorative or thermionic coatings. After a review of physical vapor deposition (PVD) techniques used for the deposition of these coatings, a survey of investigations to apply these coatings is given. As a result of the strong directionality of covalent boron–boron bonds, boride coatings show an increasing tendency to amorphous film growth with increasing B/*Me* atomic ratio and, for rare-earth hexaborides, with decreasing metallic radius of the rare-earth metal. Mechanical and optical properties are strongly influenced by the crystallographic structure of the boride phase. Because of their high hardness combined with good adhesion, crystalline films based on the diborides of transition metals seem to be promising candidates for wear resistant coatings on cutting tools. Alloying of these films with nitrogen by reactive PVD processes results in the formation of extremely fine-grained multiphase hard coatings with excellent tribological and corrosion behavior, thus offering new applications in the coating of engineering components. Because of their distinct colorations, some of the hexaborides of rare-earth elements may be used as decorative coatings on consumer products like wristwatch casings or eyeglass frames. Another promising field is the development of thermionic coatings based on rare-earth hexaborides, which may offer the possibility of the production of inexpensive and simple high emission filaments. © 1997 Academic Press

1. INTRODUCTION

The use of hard materials based on nitrides and carbides of transition metals to produce wear- and corrosion-resistant coatings on, e.g., tools, engineering components, or decorative items to increase the lifetime or to lend an attractive surface finish is now well accepted (1–3). However, although showing a promising combination of properties which have attracted an increasing number of investigators, the industrial application of boride-based thin films is very limited (4–6). The interest in boride coatings arises from the fact that the corresponding bulk phases show promising properties such as high hardness and chemical stability (7–9). The hexaborides of rare-earth elements are excellent thermionic emitters. In addition, some hexaborides and dodecaborides show interesting colorations ranging from purple–red to blue shades (10). Films based on these borides have been prepared by CVD (11–16), PACVD (17–19), and various physical vapor deposition (PVD) methods (20–63).

In this paper, after a survey of PVD methods used for the deposition of boride-based coatings, a review of studies is given that investigates the suitability of different borides for applications as wear- and corrosion-resistant, decorative and thermionic coatings. The interdependence between deposition conditions, microstructure, and properties of coatings based on the diborides and dodecaborides of transition metals and hexaborides of rare-earth metals is presented and discussed.

2. PVD METHODS FOR THE DEPOSITION OF BORIDE COATINGS

Because of difficulties arising from the application of boron-containing gases, PVD methods employed to deposit boride coatings are usually based on nonreactive techniques. The application of triode sputtering (30, 32, 40), dc (4, 5, 22, 33, 38, 44–61) and rf magnetron sputtering (31, 34–43), electron-beam evaporation (20–27), and arc evaporation (28, 29) for the deposition of boride coatings is reported in the literature. Because of the low electrical and thermal conductivity of boron (22) and because of the high reactivity of certain rare-earth metals with oxygen (e.g., lanthanum and cerium), most PVD processes make use of the corresponding boride as the vapor source instead of separated metal and boron sources (62, 63). High-quality boride targets (either as billets or rods for evaporation or as plates for sputtering) are usually prepared powder-metallurgically, e.g., by means of sintering or hot pressing. Typical values of the densities yielded are in the range of 70 to 85% of the theoretical density (34, 58). Thus, in combination with the high brittleness of boride compounds, the operation of these vapor sources in PVD techniques requires the observance of certain measures to avoid thermal overloading. To ensure a sufficient heat transfer from a sputtering target to the coolant, the application of suitable bonding techniques of the target onto the backing plate is necessary. Nevertheless, for sputtering and evaporation methods, the power applied to the target has to be limited to moderate values to

0022-4596/97 $25.00

avoid cracking or source material explosion due to localized overheating. In magnetron sputtering, the reported power densities are between 2 and 10 W cm^{-2} (4, 39–42, 46, 46–61). The resulting deposition rates vary between 1.5 and 200 nm min^{-1} for magnetron sputtering and electron-beam evaporation, respectively (4, 25, 34, 39–41, 46–61). However, values of up to 1800 nm min^{-1} are reported for arc evaporation of LaB_6 (28). For comparison, typical growth rates for TiN coatings deposited onto tools or decorative coatings range from 20 to 250 nm min^{-1} (2, 3).

The results discussed in this paper are from boride coatings deposited by conventional and unbalanced dc magnetron sputtering in the author's department with thicknesses between 2 and 5 μm. To date, there is no known industrial utilization for PVD coatings based on borides. So the following review has to be restricted to results obtained on a laboratory scale. However, from the process point of view, up-scaling of these deposition methods to the industrial scale seems to be possible.

3. STRUCTURE AND PROPERTIES OF BORIDE COATINGS

Among the deposition parameters of PVD methods, the kinetic energy of the condensing particles plays a crucial role for the growth of boride coatings—affecting both microstructure and properties. Thus the following section concentrates mainly on the influence of the argon pressure during deposition affecting the scattering processes of sputtered energetic particles (64). The targets and the deposition parameters used in this work are summarized in Table 1.

3.1. Relationships between Deposition Conditions and Microstructure

As a result of the strong directionality of the covalent boron-boron bonds (7), coatings based on borides show a pronounced tendency to form extremely fine-grained to amorphous structures if low-temperature PVD processes are used (65). The actual microstructure of boride coatings as revealed by scanning (SEM) or transmission electron microscopy (TEM) has so far only been reported for a few cases. Hence, it is not possible to draw a generic conclusion. However, in evaporation as well as in sputtering, similar results are obtained. Figure 1 shows SEM fracture cross sections of coatings deposited using sputtering from TiB_2, LaB_6, CeB_6, and ZrB_{12} targets, respectively. Deposition conditions with moderate energetic contribution for film growth seem to promote the formation of a dense, extremely fine-columnar structure (see Figs. 1a and 1c). Typical grain sizes for this structure type revealed from X-ray diffraction (XRD) measurements on ZrB_2- and LaB_6-based films were found to be below 40 nm for electron-beam evaporation (21) and below 20 nm (21, 30, 48) for sputtering. In the complementary growth region, i.e., extremely low or high energetic contribution (e.g., high argon pressure, low substrate temperature or high bias voltage, respectively) and due to the addition of nitrogen using reactive PVD processes, the structure of the coatings becomes extremely fine-grained to amorphous (see Figs. 1b and 1d). Obviously, columnar film growth requiring long-range diffusion processes is not possible at low substrate temperature (23, 25, 30), with the low energies of condensing target atoms (at high argon pressures (57–59)), during high energy ion bombardment (at high bias voltages (57–59)) or due to the addition of foreign elements (4, 5, 18, 19, 29, 35–39, 46, 47–49, 53, 58, 60, 61).

TABLE 1
Sputtering Parameters Used for the Targets Investigated

Target	Sputtering power density (W cm^{-2})	Total pressure (Pa)	Bias voltage (−V)	Substrate temperature (°C)
TiB_2[a]	2.3	0.7	100	300
ZrB_2[b]	2.8	1.1	200	300
LaB_6[b]	4.8	3	100	200
CeB_6[b]	4.8	3	100	200
SmB_6[b]	4.8	3	100	200
YB_6[b]	4.8	3	100	200
ZrB_{12}[b]	2.8	1.1	200	200

[a] Unbalanced dc magnetron sputtering.
[b] Conventional dc magnetron sputtering.

The dependence of the chemical composition of the coatings on the argon pressure is plotted as a B/*Me* atomic ratio (*Me* = metal titanium, zirconium, lanthanum, cerium, samarium or yttrium, respectively) in Fig. 2. In general, in nonreactive sputter processes, stoichiometric deviations of the coating from the target composition are attributable to interactions of the sputtered target atoms with the plasma discharge in the transport phase and at the surface of the growing film, assuming that diffusion processes in the target are inhibited (66). Therefore, the main reasons for the observed influence of the argon pressure on the chemical composition of the coatings are collisions of sputtered energetic particles with argon atoms. These collisions may be characterized by both the collision cross sections σ and the energy transfer coefficients ε. Special attention should therefore be paid to the particle radii determining the collision cross sections and to the atomic masses determining the energy transfer coefficients (67, 68). The energy transfer coefficient

$$\varepsilon = \frac{4 m_t m_{Ar}}{(m_t + m_{Ar})^2}, \qquad [1]$$

where m_t and m_{Ar} are the atomic masses of the target and argon atoms, gives the following values for collisions of the

target atoms involved with argon: $\varepsilon_{Ti} = 0.99$, $\varepsilon_{Zr} = 0.85$, $\varepsilon_{La} = 0.69$, $\varepsilon_{Ce} = 0.69$, $\varepsilon_{Sm} = 0.66$, $\varepsilon_{Y} = 0.86$, and $\varepsilon_{B} = 0.67$. Considering the low particle radius and thus low collision cross section of boron atoms, we can assume boron atoms to have a high mobility within the discharge at low pressures thus comparatively easily arriving at the substrate. This interpretation is suitable to explain the overstoichiometry of the coatings sputtered from all targets with the exception of ZrB_{12} (52) (compare Fig. 2).

With increasing argon pressure we have to distinguish in more detail between the behavior of the sputtered particles in the discharge. Taking into account momentum and energy conservation during elastic collisions, boron atoms colliding with argon atoms at high process gas pressures are expected to preferentially recoil with respect to their original movement direction. This has been confirmed by Monte Carlo simulations of the behavior of sputtered lanthanum and boron atoms (45), which show that with increasing pressure an increasing number of boron atoms is thermalized and thus has reduced deposition probabilities (69). However, the effect of this mechanism is superposed by the high particle radius and thus collision cross section of titanium and zirconium atoms combined with the efficient energy transfer to argon atoms expressed by ε, resulting in very low deposition probabilities for titanium and zirconium atoms at high argon pressures. These considerations explain the increase in the B/Zr atomic ratio with increasing pressure for both the ZrB_2 and ZrB_{12} targets. In contrast to that, the rare-earth atoms are not so affected by scattering because of their high atomic masses with respect to argon and the resulting lower value for the energy transfer coefficient ε. These interpretations are in good agreement with other investigations concerning diboride (4, 13, 14) and lanthanum hexaboride coatings (41, 45).

The addition of nitrogen during the sputtering process results in an increasing nitrogen concentration within the coating at the expense of the boron content. More detailed information can be found in Refs. (4, 5, 18, 19, 29, 35–39, 46, 47–49, 53, 58, 60, 61).

Typical XRD traces of coatings deposited onto molybdenum substrates are shown in Figs. 3 and 4. In the case of nonreactive sputtering from TiB_2 or ZrB_2 targets, films containing the hexagonal TiB_2 or ZrB_2 phases, respectively, were deposited (Figs. 4a and 4b). Within the range of the deposition parameters investigated, a pronounced (001) texture of the TiB_2 phase and a weak (001) texture to an almost random orientation of the ZrB_2 phase determined from texture coefficients (70) was observed. In diboride films with low nitrogen concentrations the corresponding diboride phase is still present (see Fig. 3c) (4, 5, 18, 19, 29, 35–39, 47–49, 53, 58). High nitrogen contents result in the formation of X-ray amorphous films, which may be regarded as having a nanocrystalline multiphase structure consisting of the corresponding diboride and nitride phases, as well as hexagonal boron nitride (4, 5, 35–37). The same considerations have been assumed for nitrogen-alloyed hexaboride coatings (49, 58). Nonreactive deposition using ZrB_{12} targets leads to the appearance of extremely broad features in the XRD traces (Fig. 3d). While the formation of an (001)-oriented ZrB_2 phase could unambiguously be detected, the additional feature centered at 37° (full width at half maximum (FWHM) approximately 11°) may be identified as originating from the rhombohedral boron phase or from a tendency to order only in the sense that atoms are fairly tightly packed together and show a statistical preference for a particular interatomic distance within a boron or boron-rich phase (52, 71, 72). No evidence of the formation of the metastable ZrB_{12} phase (73) was detected.

A rough interpretation of the tendency to form the corresponding hexaboride phase during deposition may be given by the consideration of the size of the rare-earth atom that is appropriate to the metallic sites in the rigid boron skeleton (7, 9). For hexaborides, the metallic radii for the rare-earth atom may vary between 0.175 and 0.223 nm (10). Following the different radii for lanthanum (0.1870 nm), cerium (0.1825 nm), samarium (0.1802 nm), and yttrium (0.1776 nm), a decreasing tendency to stabilize the crystalline hexaboride phase in sputtered films is observed (Fig. 4). Despite the broad composition range observed (compare Fig. 2), other rare-earth boride phases could not be detected. For crystalline films, the preferred orientation of the hexaboride phase is (100) (6, 21, 22, 26, 34, 41, 42, 50, 51, 55–59). With increasing kinetic energy of the condensing target atoms, a change in the texture from (100) to (110) and (111) is observed (6, 41, 45, 55, 57–59), which is related to different contributions of the strain and surface energy of the films. Nakano *et al.* (42) calculated the strain energy for different faces of the LaB_6 lattice to increase in the order (111) < (110) < (100), while the surface energy shows the opposite trend. As the contribution of kinetic particles to film growth increases, the contribution of the strain energy becomes dominant and, consequently, the preferred (100) orientation vanishes.

For TiB_2-based coatings the lattice parameter c of the TiB_2 phase shows a weak decrease from 0.322 to 0.320 nm with increasing argon pressure corresponding to distortions of -0.23 to -0.85% with respect to the literature value of TiB_2 ($c = 0.32295$ nm (74)). The strong (001) texture prevents the calculation of the a value. The lattice parameters of the ZrB_2 phase vary without pronounced tendency in the range of $a = 0.320$ to 0.321 nm and $c = 0.345$ to 0.346 nm. These values correspond to lattice distortions in the a direction of $+0.91/+1.30\%$ and parallel to the c axis of $-1.28/-2.19\%$ as compared with the bulk values of ZrB_2 ($a = 0.3168$ nm and $c = 0.3530$ nm (74)). For the hexaboride phases in PVD coatings, lattice parameters determined by XRD techniques between 0.416 and 0.422 nm for LaB_6, 0.415 and 0.418 nm for CeB_6, and 0.417 and 0.421 nm for SmB_6 are found; this corresponds to distortions from the

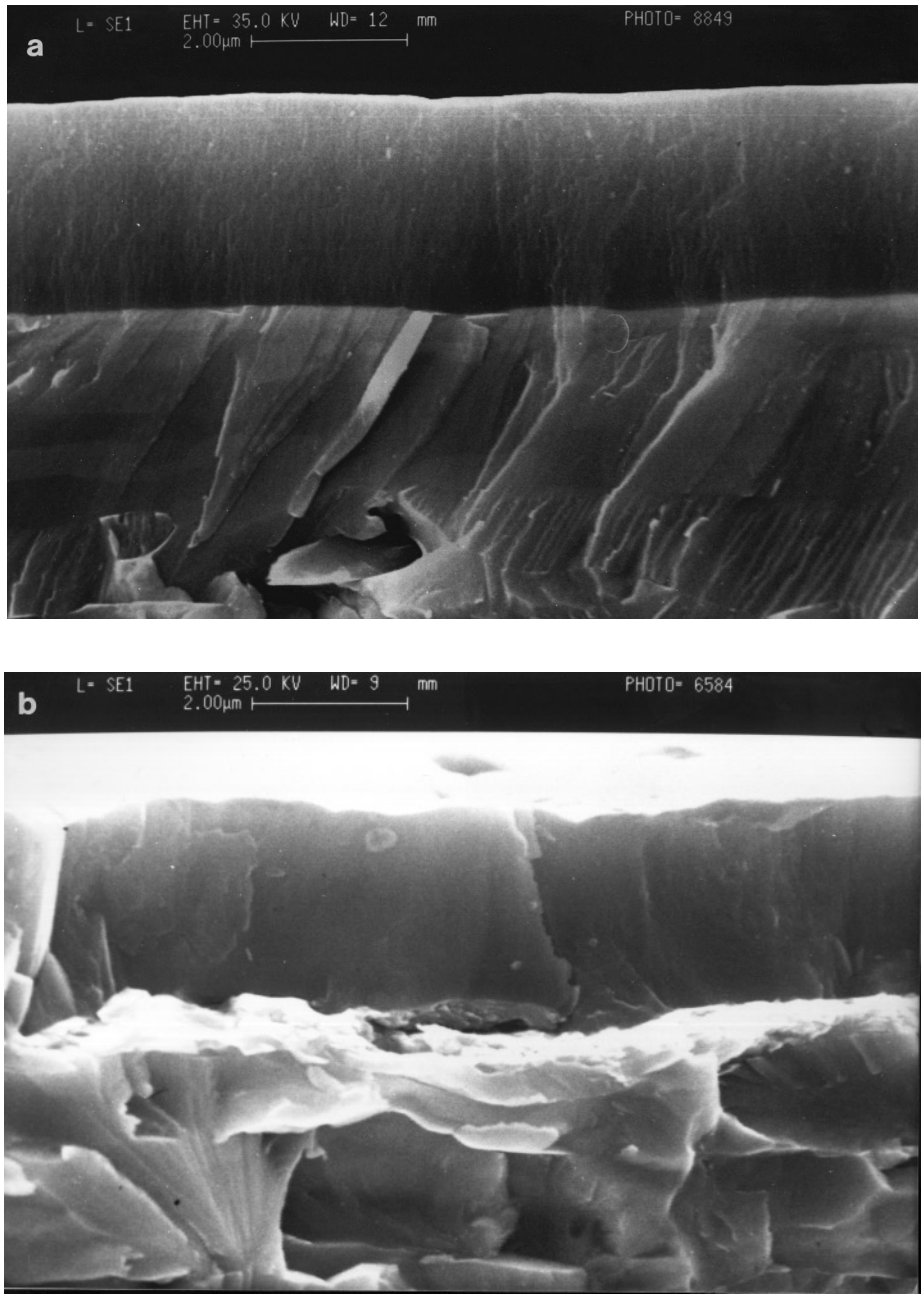

FIG. 1. Cross-sectional SEM micrographs of boride coatings sputtered nonreactively from different targets (deposition parameters see Table 1). (a) target: TiB_2. (b) target: LaB_6. (c) target: CeB_6. (d) target: ZrB_{12}.

standard value of the bulk phases (LaB_6, $a = 0.4153$ nm; CeB_6, $a = 0.4141$ nm; SmB_6, $a = 0.4133$ nm (74)) of $+0.17$ to $+1.61\%$, $+0.22$ to $+0.94\%$, and $+0.89$ to 1.86%. In agreement with the considerations above, the highest values for the lattice parameter were obtained for sputtering at low process gas pressures (6, 41, 55, 57–59). These distortions are on the one hand attributed to the effect of excess boron (compare Fig. 2) which may be incorporated interstitially in the boride lattice, or on the other hand to the incorporation of argon atoms (75) or impurities originating from residual gases during the deposition process.

3.2. Relationships between Microstructure and Properties

3.2.1. Film hardness and adhesion. The crystallographic structure established by the rigid boron skeleton is expected

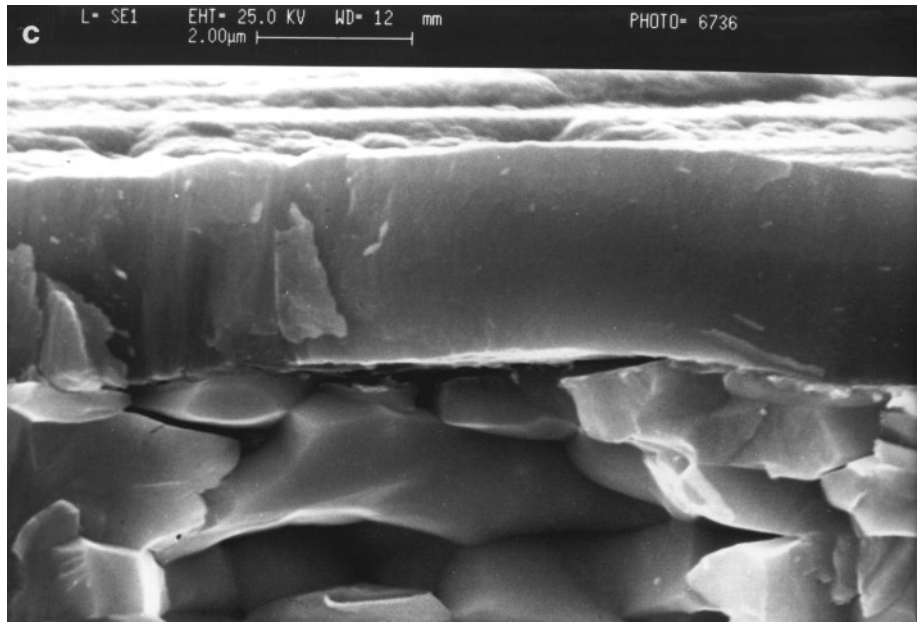

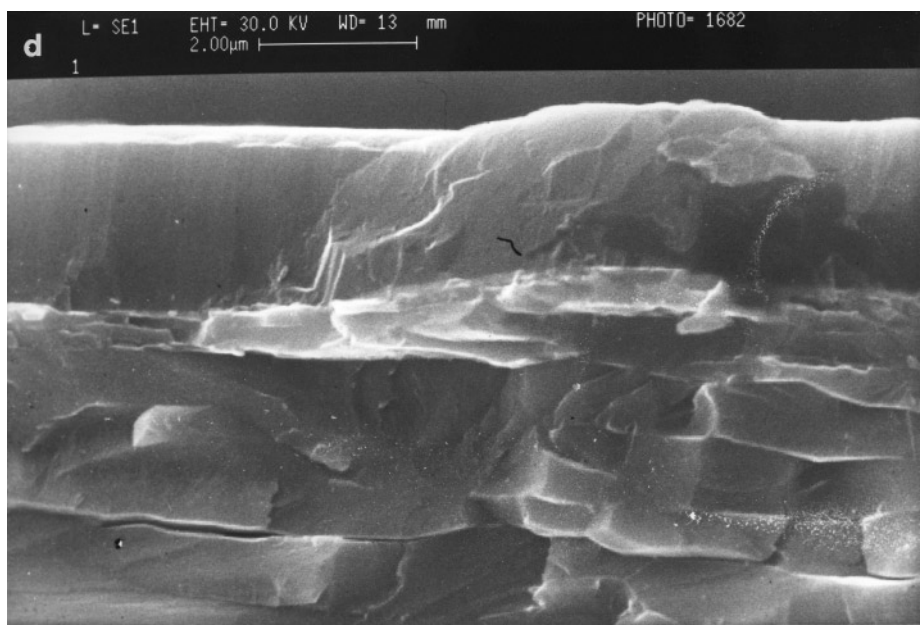

FIG. 1—*Continued*

to determine the film hardness rather than the chemical composition of most boride coatings (6, 57). Especially for those coatings with distinct covalent binding character, i.e., hexaborides and dodecaborides, the adhesion to metallic substrates seems to cause serious difficulties in the application of these films (6, 21, 27, 28, 34, 50–52, 55–57). Due to the similarities existing between the rare-earth hexaborides, a more detailed interpretation of the interrelationships between the coating microstructure and the hardness is possible. For diboride films, however, a serious discussion is prevented due to the hexagonal lattice formed with distinct preferred orientation (compare Fig. 3) and the marked differences between the bulk hardness values of TiB_2 (3480 HV (76)) and ZrB_2 (2200 HV (76)).

In Fig. 5, Vickers microhardness values of boride coatings with crystalline structure are plotted as a function of the lattice distortion. The hardness of those coatings sputtered from the ZrB_2 target shows a good agreement with the

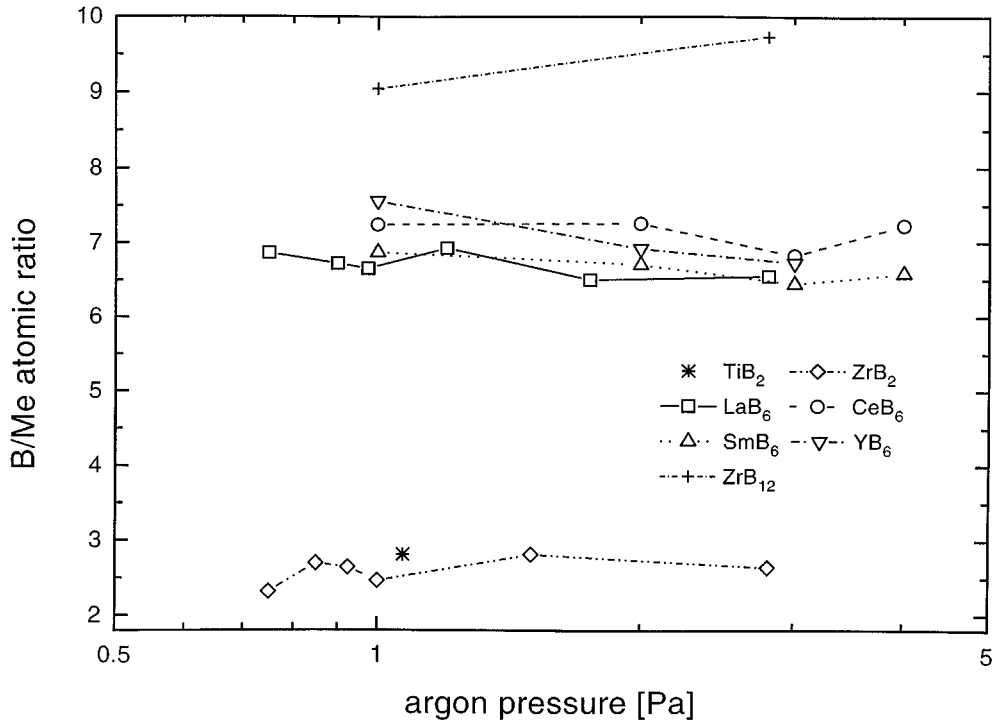

FIG. 2. Dependence of the chemical composition of sputtered boride coatings on the argon pressure (deposition parameters see Table 1).

corresponding bulk value. In contrast to that, TiB_2-based coatings with reported hardness values in the range of 3000 to 7000 HV (4, 5, 18, 19, 29, 35–39) are regarded as ultrahard coatings. These high values are expected to be the result of the dense, extremely fine-columnar structure (compare Fig. 1a) and high compressive stresses (up to 4 GPa (4)). For hexaboride coatings with lattice parameters close to the literature value (and B/*Me* atomic ratios close to stoichiometry, see Fig. 2), hardnesses well below the bulk values (LaB_6, 2600 HV50; CeB_6, 2550 HV50; SmB_6, 2520 HV50; YB_6, 2550 HV50 (10)) are observed. These low hardness values may be caused by deposition conditions with low particle energies and low substrate temperatures promoting the formation of low-strength grain boundaries due to incomplete coalescence between growing crystals (77). In extremely fine-grained to fracture-amorphous structures the well-known Hall–Petch relation valid for comparatively large grain sizes may therefore be overlapped by the high density of grain boundaries and voids (75). In addition, internal stress can be relaxed at open-voided grain boundaries. The low hardness values obtained are therefore attributed to the observed extremely fine-grained to fracture-amorphous structure with low-strength grain boundaries.

The maximum hardness values shown in Fig. 5 for lattice distortions between + 0.5 and + 1.5% are attributed to the formation of fine-columned films with strong grain boundaries. However, since stress relaxation is not possible, the highest compressive stresses with values up to 2.7 GPa are reported for this film type (42). Consequently, these high stress levels impose strong requirements on the adhesion strength of the films, which may not be satisfied in every case (6, 21, 27, 28, 34, 50, 51, 55–57).

The highest distortion values corresponding to decreasing hardness are observed in those coatings with increasing amorphous character, i.e., coatings based on SmB_6, YB_6, and ZrB_{12} (compare Figs. 3 and 4, the hardness values of coatings sputtered from YB_6 and ZrB_{12} targets range between 1700 and 1800 HV0.01 (51) and 1400 and 2200 HV0.01 (49, 52, 58), respectively). This is due to the decreasing grain size and the increasing role of grain boundary material preventing the explanation of mechanical properties by dislocation theory. For these nanocrystalline or amorphous films, an inverse Hall–Petch relationship has been established under the assumption that the yield strength and elastic constants of interfaces are lower than those of crystalline material (5).

With increasing nitrogen concentration within the coatings, a decreasing hardness is observed (4, 5, 29, 38, 47, 49, 57–59) corresponding to the increasing relative amount of the softer nitride and the hexagonal boron nitride phase. For these multiphase films with high nitrogen contents hardness values in the range between 700 and 2000 HV0.01 have been observed (4, 5, 35–39, 47, 49, 57–59).

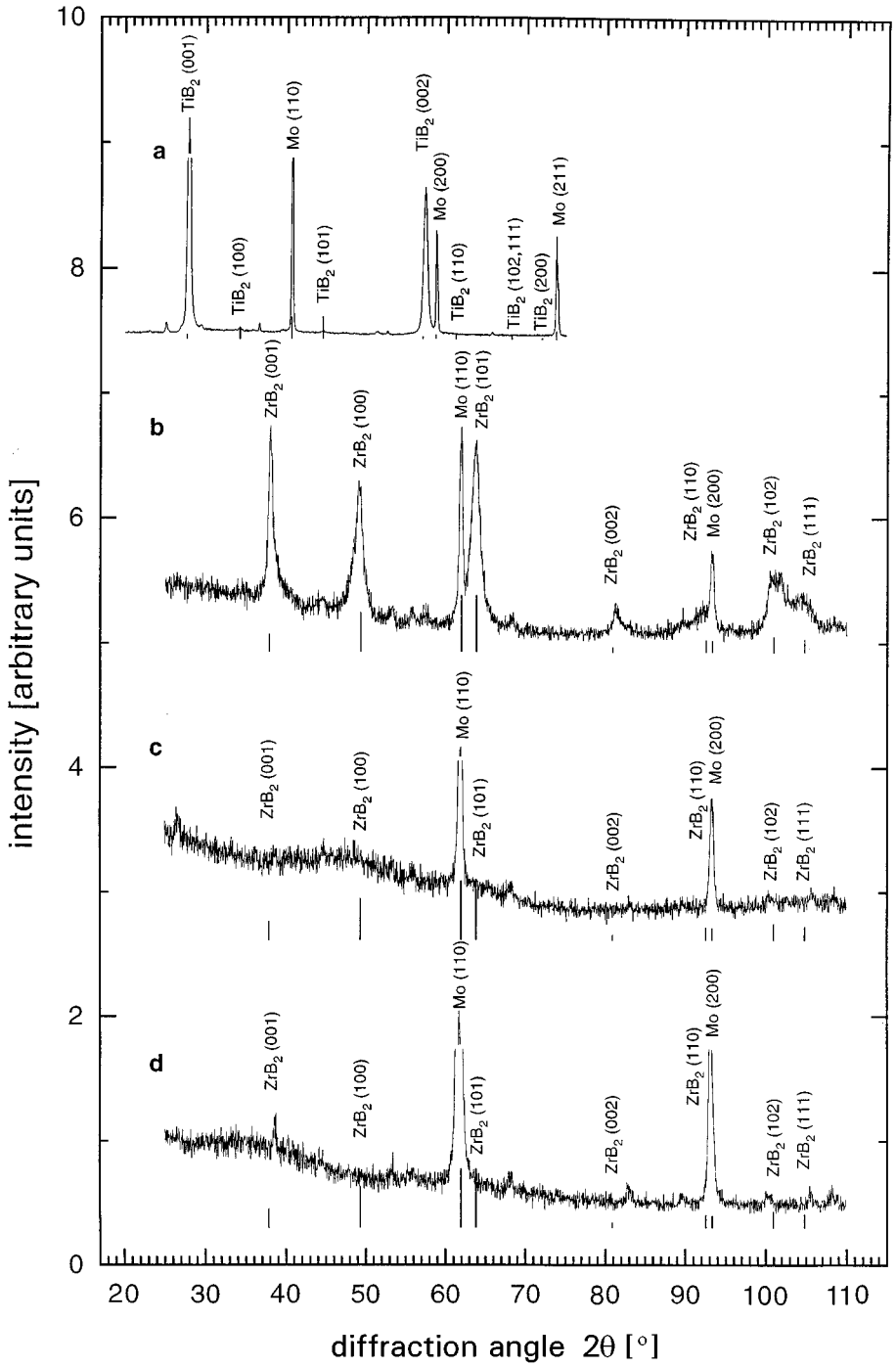

FIG. 3. X-ray diffraction spectra of sputtered boride coatings (substrate, molybdenum; deposition parameters see Table 1). (a) target: TiB_2 (copper $K\alpha$ radiation). (b) target: ZrB_2 (chromium $K\alpha$ radiation). (c) target: ZrB_2 (chromium $K\alpha$ radiation; film nitrogen content, 8 at.%). (d) target: ZrB_{12} (chromium $K\alpha$ radiation).

3.2.2. Tribological properties. Due to the formation of multiphase films consisting of hard and soft lubricating phases during reactive sputtering, nitrogen-containing diboride-based coatings seem to be promising candidates for tribological applications (5, 29, 39, 46, 77, 78). Figure 6 shows the wear coefficient of nitrogen-alloyed ZrB_2-based coatings determined by a block-on-cylinder test using coated Ck45 substrates as blocks and uncoated Ck45 cylinders in an oil-lubricated condition as a function of the nitrogen content (78). In all cases the wear coefficient was

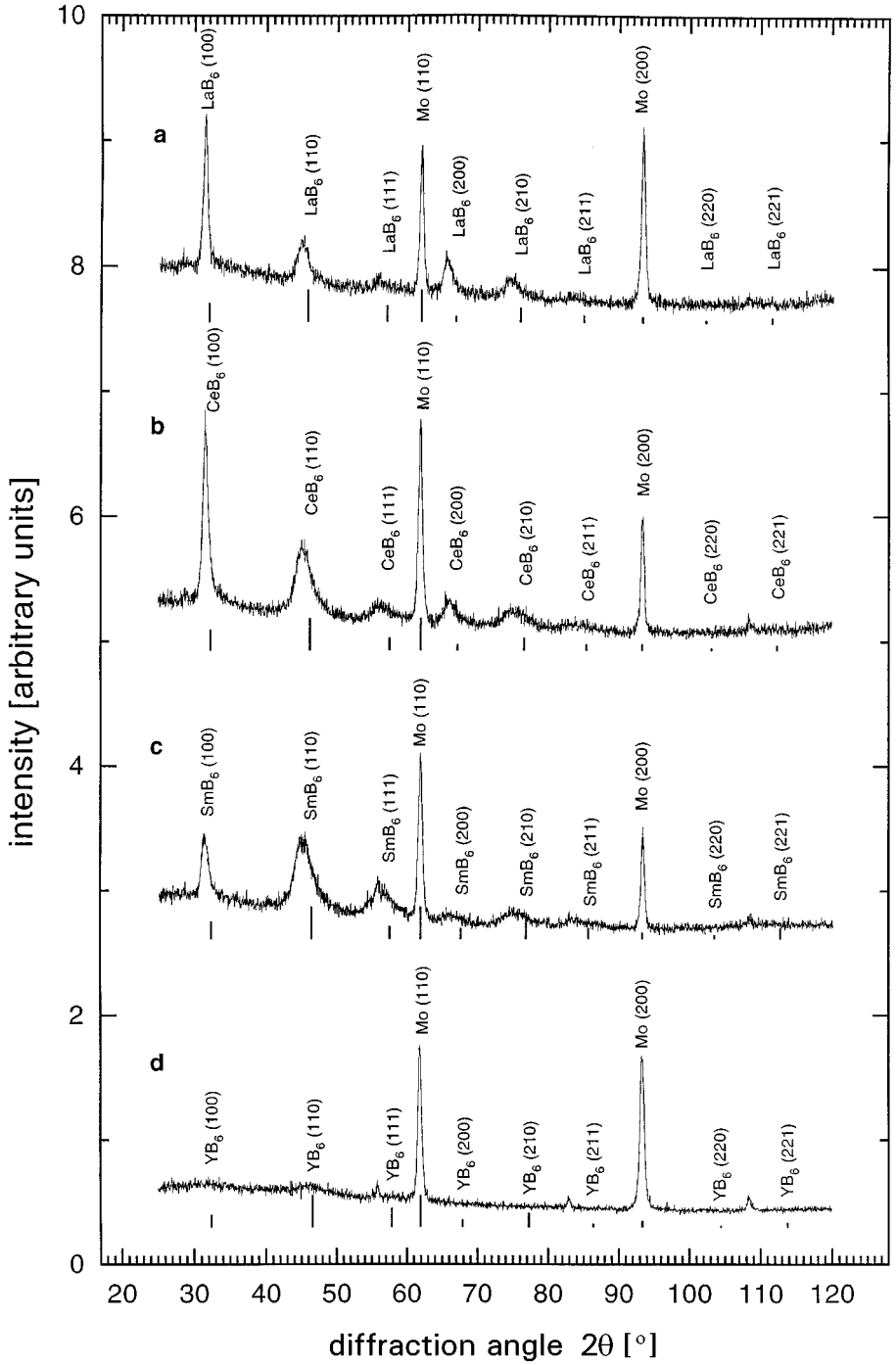

FIG. 4. X-ray diffraction spectra of sputtered rare-earth hexaboride coatings (substrate, molybdenum; chromium $K\alpha$ radiation; deposition parameters see Table 1). (a) target: LaB_6. (b) target: CeB_6. (c) target: SmB_6. (d) target: YB_6.

significantly lowered by the coating with respect to uncoated samples ($k_v = 1329\ \mu m^4\ min^{-1}$). Despite the fact that the film hardness is decreasing with increasing nitrogen concentration (compare Section 3.2.1.), a marked decrease of the wear coefficient was observed for low nitrogen contents. This decrease is attributed to the transition in the film structure from the fine-columnar ZrB_2 phase to the nanocrystalline multiphase structure (46). For this structure type friction coefficients against steel as low as 0.15 are reported (29). Very high nitrogen concentrations lead to an increase

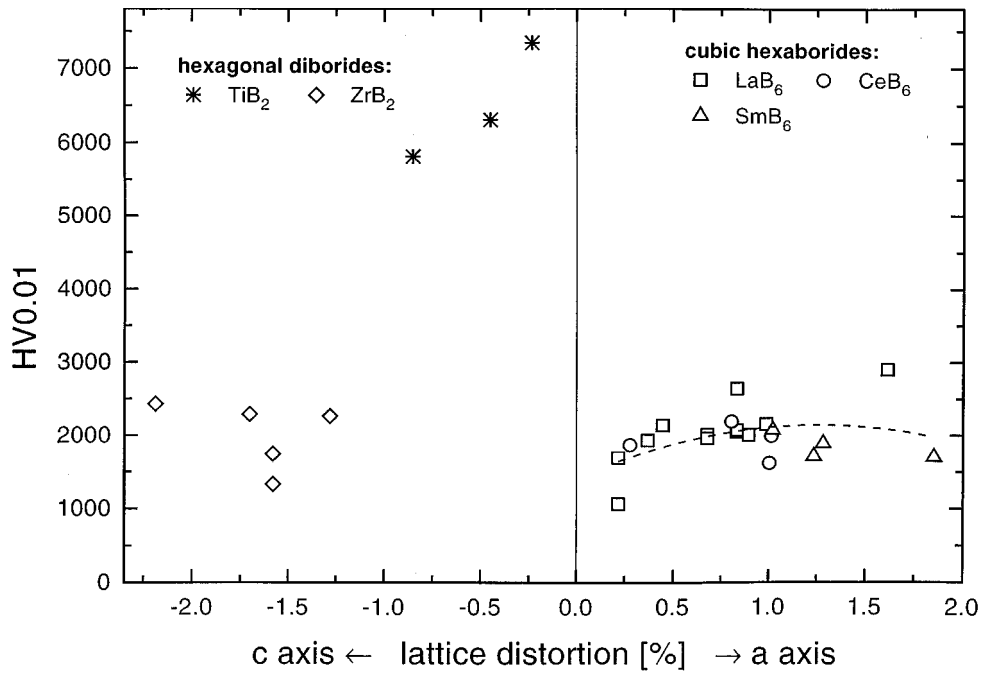

FIG. 5. Relationship between Vickers microhardness HV0.01 and lattice distortion of sputtered boride coatings (deposition parameters see Table 1).

in the wear coefficient due to the increasing amount of hexagonal boron nitride within the films.

3.2.3. Corrosion behavior. The high chemical stability and the dense structure makes diboride coatings interesting candidates for applications in severe corrosive mediums (29, 53, 54, 79). Potentiodynamic polarization measurements of coated Ck35 substrates in 1 *N* sulfuric acid showed far better electrochemical behavior of nitrogen alloyed ZrB_2-based coatings with respect to unalloyed coatings and

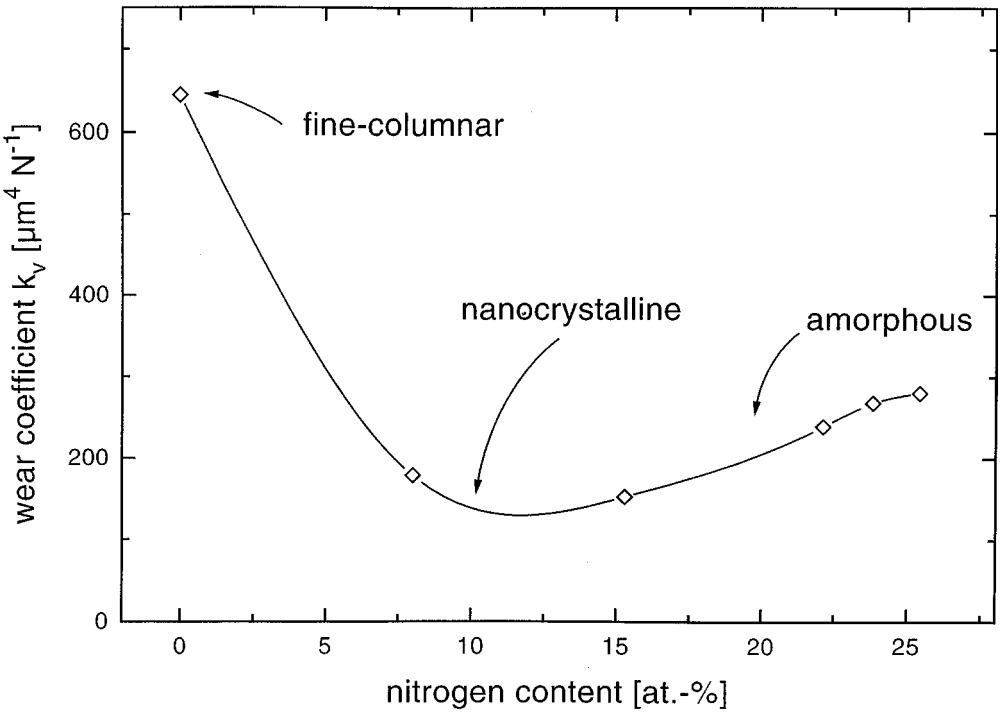

FIG. 6. Dependence of the wear coefficient of sputtered Zr–B–N coatings on the nitrogen content (deposition parameters see Table 1).

uncoated samples by decreasing the active corrosion rate, the critical current density, and the minimum passive current (54). However, due to the formation of microscopic (i.e., pinholes) and macroscopic defects (i.e., craters and droplets) in PVD coatings (54, 80, 81), the substrate surface is not covered entirely without physical discontinuities. Using electrochemical impedance spectroscopy measurements in 1 *N* sulfuric acid (82), for unalloyed and nitrogen-alloyed ZrB_2-based coatings (nitrogen-concentration, 22 at.%) porosities of 0.67 and 0.021%, respectively, were obtained (54). This behavior is correlated with the fine-columnar structure favoring voided grain boundaries in unalloyed films and with the dense, fracture-amorphous structure of nitrogen-alloyed coatings (compare Fig. 1). Similar results have been obtained by Aromaa *et al.* (79) for TiB_2-based coatings.

In contrast to the results described above, unalloyed ZrB_2-based coatings deposited to austentitic stainless steel substrates showed a better corrosion resistance than nitrogen-containing coatings which failed due to decomposition (53). By combination of the beneficial properties of both coating types, i.e., high hardness and good inherent chemical stability of ZrB_2 coatings and dense structure of nitrogen–alloyed films, in multilayers the number of defective sites has been significantly reduced and thus a marked improvement of the corrosion resistance of base substrate metals is possible (83).

TABLE 2
CIE-$L^*a^*b^*$ Colourimetric Indexes of Various Sputtered Boride Coatings

	L^*	a^*	b^*
$ZrB_{1.49}N_{0.68}$	50	3	−2
LaB_6	37 … 52	5 … 8	−6 … −12
CeB_6	44 … 46	3 … 4	−4 … −5
SmB_6	45 … 47	3 … 4	−2 … −3
YB_6	62 … 65	2 … 4	0 … −1

3.2.4. Optical properties. Table 2 summarizes the CIE-$L^*a^*b^*$ colorimetric indexes (84) for those boride coatings (6, 47, 49, 50–53, 57–59) representing promising candidates for decorative applications. For nitrogen-alloyed ZrB_2-based coatings, a dark gray coloration was observed. Corresponding to the formation of the ZrB_2 phase in films sputtered from the ZrB_{12} target, these coatings show a silver–gray surface. For hexaboride films, the visual impression of the corresponding bulk materials with more distinct color components was not obtained. The most marked color impression was obtained for LaB_6-based coatings corresponding to dark violet. Following the tendency to form amorphous film structure (compare Fig. 4), a decrease

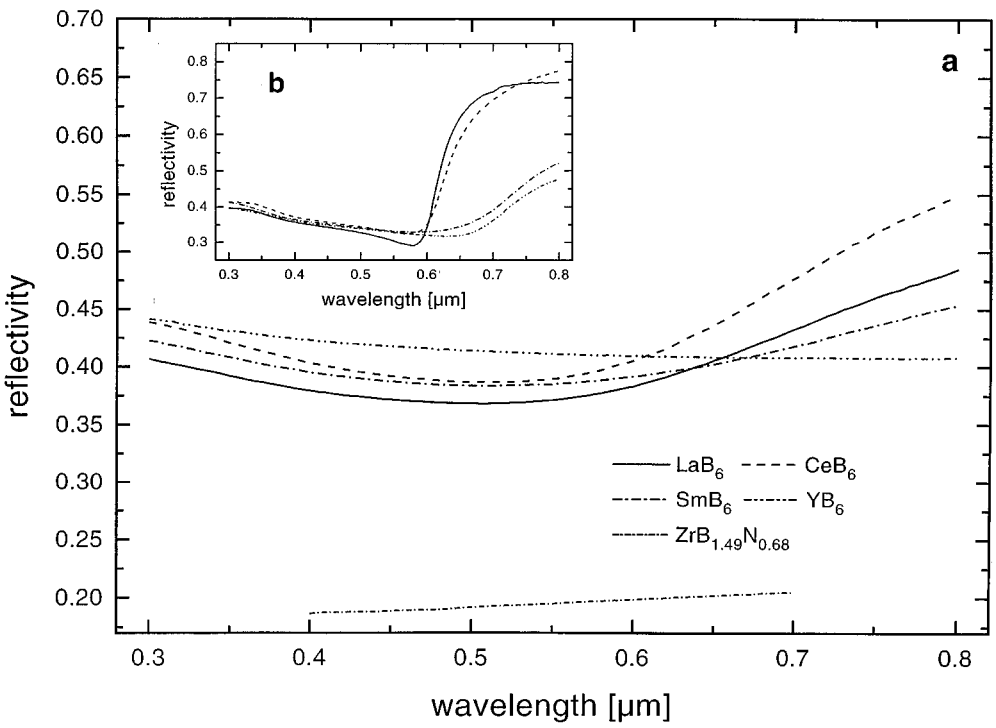

FIG. 7. Spectral reflectivity calculated from ellipsometric data (angle of incidence, 75°) of (a) sputtered boride coatings (deposition parameters see Table 1) and (b) the bulk materials LaB_6, CeB_6, SmB_6, and YB_6

in the color components a^* and b^* was observed. YB_6-based films exhibit a silver–gray appearance.

Colorations generated by interactions of bound and/or free electrons with the incident light depend on the crystal structure and the chemical composition of the material. A more detailed understanding of the origins of colorations in decorative coatings can be obtained by spectroscopic ellipsometry (3, 85). Figure 7 shows the spectral reflectivity calculated from ellipsometric data for boride coatings and for the corresponding bulk hexaborides. Due to the highly disordered microstructure of these coatings, their electronic and, consequently, their optical properties differ from those of the bulk values (21, 30, 86–89). Structural defects like interstitials, vacancies, and impurities which are typical for coatings grown by low-temperature PVD processes are expected to affect the shape of the plasma oscillation edge in rare-earth hexaborides (90). This has been confirmed by Peschmann *et al.* (21), who calculated reduced electron mean free paths and relaxation times due to increased electron scattering for LaB_6-based coatings. Nitrogen-alloyed ZrB_2-based coatings show an almost wavelength-independent reflectivity of about 0.2.

3.2.5. Thermionic emission. Films based on rare-earth hexaborides may be interesting candidates for thermionic emitters (91). Figure 8 shows the emission current of coated and uncoated tungsten cathodes as a function of the filament temperature. As can be clearly seen, coated filaments work at temperatures approximately 1000°C below the operating temperature of an uncoated tungsten filament while emitting nearly the same electron current. The work functions at temperatures ranging from 900 to 1100°C were calculated from Richardson plots to $\phi_{LaB_6} = 2.64$ eV, $\phi_{CeB_6} = 3.27$ eV, $\phi_{SmB_6} = 3.11$ eV, and $\phi_{YB_6} = 3.05$ eV (55, 56). These values are in good agreement with those reported for bulk cathodes (91).

5. CONCLUSIONS

This paper has reviewed PVD techniques for the deposition of coatings based on various borides and the interrelationships between deposition conditions, microstructure, mechanical, and application-related properties. Although no industrial applications of these coatings is known at present, they are promising candidates for several applications:

(i) Because of their high hardness and good chemical stability, coatings based on the diborides of the transition metals may be applied for the protection of tools and engineering components in conditions of extreme mechanical wear and/or severe corrosion. Alloying of these coatings with nitrogen improves their tribological properties significantly.

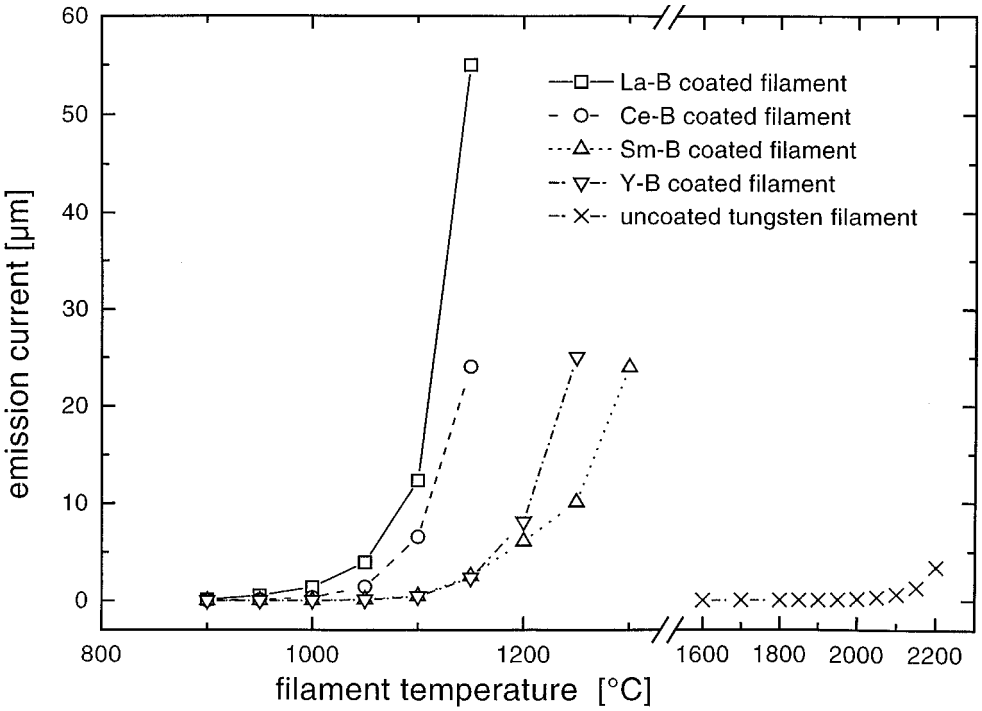

FIG. 8. Dependence of the emission current of uncoated and coated tungsten filaments on the operating temperature (deposition parameters see Table 1).

(ii) Although the fascinating optical properties of the corresponding bulk materials could not be realized completely due to different microstructure and thus electronic properties, especially LaB_6-based coatings provide an opportunity to expand the existing chromatic spectrum of decorative hard coatings to violet tones. Nitrogen-alloyed ZrB_2-based films may be applied as anthracite-colored decorative coatings with excellent corrosion resistance.

(iii) Rare-earth hexaboride coatings offer the possibility of the production of low-cost electron emitters due to their low values of the work function.

ACKNOWLEDGMENTS

The author is grateful to his co-workers G. Hawranek, E. Kelesoglu, J. Komenda-Stallmaier, P. Losbichler, A. Übleis, and Dr. W. Waldhauser at the Institut für Metallkunde und Werkstoffprüfung, Montanuniversität Leoben for their help in film deposition and characterization. He also thanks Professor H. Störi and his co-workers at the Institut für Allgemeine Physik, Technische Universität Wien for conducting the film analyses, Dr. P. Rödhammer (Metallwerk Plansee, Reutte) for supplying the molybdenum sheets, and Dr. H. Baumann (Institut für Kernphysik, Universität Frankfurt) for RBS and ERD analysis. Dr. F. Vollertsen (Lehrstuhl für Fertigungstechnologie, Universität Erlangen) and Professor M. Ürgen (Department of Metallurgical Engineering, Istanbul Technical University) are acknowledged for the characterization of the wear and corrosion behavior. The author is also grateful to Dr. U. Beck and Professor G. Reiners (Bundesanstalt für Materialforschung und -prüfung, Berlin) for their assistance in conducting the optical characterization of the coatings. Parts of this project were supported by the Ministerium für Forschung, Verkehr und Kunst (Contracts GZ. 49.915 and GZ 49.868), the Jubiläumsfonds der Oesterreichischen Nationalbank (Project 5196), and the Fonds zur Förderung der wissenschaftlichen Forschung (Project P 10 764 ÖTE).

REFERENCES

1. W. Schintlmeister, and O. Pacher, *J. Vac. Sci. Technol.* **12,** 743 (1975).
2. J. Vogel and E. Bergmann, *J. Vac. Sci. Technol. A* **6,** 2431 (1986).
3. G. Reiners, U. Beck, and H. A. Jehn, *Thin Solid Films* **253,** 33 (1994).
4. C. Mitterer, M. Rauter, and P. Rödhammer, *Surf. Coat. Technol.* **41,** 351 (1990).
5. W. Gissler, *Surf. Coat. Technol.* **68/69,** 556 (1994).
6. C. Mitterer, W. Waldhauser, U. Beck, and G. Reiners, *Surf. Coat. Technol.* **86/87,** 715 (1996).
7. J. Etourneau and P. Hagenmüller, *Philos. Mag.* **52**(3), 589 (1985).
8. F. Binder, *Radex-Rundschau* **4,** 531 (1975).
9. K. A. Schwetz, K. Reinmuth, and A. Lipp, *Radex-Rundschau* **3,** 568 (1981).
10. F. Binder, *Radex-Rundschau* **1,** 52 (1977).
11. H. O. Pierson and E. Randich, *Thin Solid Films* **54,** 119 (1978).
12. H. O. Pierson, E. Randich, and D. M. Mattox, *J. Less-Common Met.* **67,** 381 (1979).
13. H. O. Pierson and A. W. Mullendore, *Thin Solid Films* **72,** 511 (1980).
14. H. O. Pierson and A. W. Mullendore, *Thin Solid Films* **95,** 99 (1982).
15. E. Randich and D. D. Allred, *Thin Solid Films* **83,** 393 (1981).
16. S. Motojima, K. Funahashi, and K. Kurosawa, *Thin Solid Films* **189,** 73 (1990).
17. L. M. Williams, *Appl. Phys. Lett.* **46**(1), 43 (1985).
18. H. Störi, H. Karner, J. Laimer, and P. Rödhammer, *Surf. Coat. Technol.* **39/40,** 293 (1989).
19. J. Laimer, H. Karner, H. Störi, and P. Rödhammer, *in* "Plasma Properties, Deposition and Etching" (J. J. Pouch and S. Alterowitz, Eds.), Vol. 140–142, p. 493, Materials Science Forum. Transtech Publications, Aedermannsdorf, 1993.
20. R. F. Bunshah, R. Nimmagadda, W. Dunford, B. A. Movchan, A. V. Demchishin, and N. A. Chursanov, *Thin Solid Films* **54,** 85 (1978).
21. K. R. Peschmann, J. T. Calow, and K. G. Knauff, *J. Appl. Phys.* **5,** 2252 (1973).
22. J. G. Ryan and S. Roberts, *Thin Solid Films* **135,** 9 (1986).
23. J. G. Ociepa and S. Mróz, *Thin Solid Films* **85,** 43 (1981).
24. J. G. Ociepa, *Thin Solid Films* **120,** 123 (1984).
25. C. Oshima, S. Horiuchi, and S. Kawai, *Jpn. J. Appl. Phys.* **2**(1), 281 (1974).
26. A. Yutani, A. Kobayashi, and A. Kinbara, *Appl. Surf. Sci.* **70/71,** 737 (1993).
27. T. Mori, K. Akaishi, Y. Kubota, O. Motojima, M. Mushiaki, Y. Funato, and Y. Hanaoka, *J. Nucl. Mater.* **200,** 385 (1993).
28. A. A. Kondrashin, V. N. Cherynaev, V. F. Korzo, and V. G. Blokhin, *Inorg. Mater.* **18,** 34 (1982).
29. M. Tamura and H. Kubo, *Surf. Coat. Technol.* **54/55,** 255 (1992).
30. S. Winsztal, H. Majewska-Minor, M. Wisniewska, and T. Niemyski, *Mater. Res. Bull.* **8,** 1329 (1973).
31. J. R. Shappirio and J. J. Finegan, *Thin Solid Films* **107,** 81 (1983).
32. U. K. Chakrabarti, H. Barz, W. C. Dautremont-Smith, J. W. Lee, and T. Y. Kometani, *J. Vac. Sci. Technol. A* **2,** 196 (1986).
33. R. Schneider, J. Geerk, and H. Rietschel, *Europhys. Lett.* **7,** 845 (1987).
34. S. Mroczkowski, *J. Vac. Sci. Technol. A* **9,** 586 (1991).
35. T. Friesen, J. Haupt, W. Gissler, A. Barna, and P. B Barna, *Surf. Coat. Technol.* **48,** 169 (1991).
36. T. Friesen, J. Haupt, W. Gissler, A. Barna, and P. B. Barna, *Vacuum,* **43**(5–7), 657 (1992).
37. T. Friesen, J. Haupt, P. N. Gibson, and W. Gissler, *in* "Mechanical Properties and Deformation Behaviour of Materials Having Ultra-Fine Microstructures" (M. Nastasi, Ed.), p. 575. Kluwer Academic, Dordrecht, 1993.
38. O. Knotek, F. Jungblut, and K. Breidenbach, *Vacuum* **7**–9, 2184 (1990).
39. W. Herr, B. Matthes, E. Broszeit, and K. H. Kloos, *Mater. Sci. Eng. A* **140,** 616 (1991).
40. K. Oda, T. Yoshio, and K. Oda, *J. Mater. Sci. Lett.* **9,** 1080 (1990)
41. T. Kajiwara, T. Urakabe, K. Sano, K. Fukuyama, K. Watanabe, S. Baba, T. Nakano, and A. Kinbara, *Vacuum* **4–6,** 1224 (1990).
42. T. Nakano, S. Baba, A. Kobayashi, A. Kinbara, T. Kajiwara, and K. Watanabe, *J. Vac. Sci. Technol. A* **3,** 547 (1991).
43. W. A. Zdaniewski, J. Wu, S. C. Gujrathi, and K. Oxorn, *J. Mater. Res.* **5,** 1066 (1991).
44. M. Mushiaki, K. Akaishi, T. Mori, Y. Kubota, Y. Funato, and O. Motojima, *Mater. Sci. Eng. A* **163,** 177 (1993).
45. A. Kinbara, T. Nakano, A. Kobayashi, S. Baba, and T. Kajiwara, *Appl. Surf. Sci.* **70/71,** 742 (1993).
46. H. Deng, J. Chen, R. B. Inturi, and J. A. Barnard, *Surf. Coat. Technol.* **76–77,** 609 (1995).
47. C. Mitterer, A. Übleis, and R. Ebner, *Mater. Sci. Eng. A* **140,** 670 (1991).
48. E. Brandstetter, C. Mitterer, and R. Ebner, *Thin Solid Films* **201,** 123 (1991).
49. C. Mitterer, P. Losbichler, W. S. M. Werner, H. Störi, and J. Barounig, *Surf. Coat. Technol.* **54/55,** 329 (1992).
50. J. Stallmaier, C. Mitterer, and J. Barounig, *Le Vide, les Couches Minces* **261,** 265 (1992).
51. W. Waldhauser, C. Mitterer, P. Schmölz, H. Störi, and J. Barounig, *in* "Proc. 13th Int. Plansee Seminar" (H. Bildstein, and R. Eck, Eds.), Vol. 4, p. 267. Reutte, 1993.
52. P. Losbichler, C. Mitterer, W. S. M. Werner, H. Störi, and J. Barounig, *Thin Solid Films* **228,** 56 (1993).

53. A. Übleis, C. Mitterer, and R. Ebner, *Surf. Coat. Technol.* **60,** 571 (1993).
54. M. Ürgen, A. F. Çakir, O. L. Eryilmaz, and C. Mitterer, *Surf. Coat. Technol.* **71,** 60 (1995).
55. W. Waldhauser, C. Mitterer, J. Laimer, and H. Störi, *Surf. Coat. Technol.* **74–75,** 890 (1995).
56. W. Waldhauser, C. Mitterer, and A. Winkler, *Le Vide: Sci. Tech. Appl.* **279,** 128 (1996).
57. C. Mitterer, J. Komenda-Stallmaier, P. Losbichler, P. Schmölz, and H. Störi, *Surf. Coat. Technol.* **74–75,** 1020 (1995).
58. C. Mitterer, J. Komenda-Stallmaier, P. Losbichler, P. Schmölz, W. S. M. Werner, and H. Störi, *Vacuum,* **11,** 1281 (1995).
59. C. Mitterer, J. Komenda-Stallmaier, P. Losbichler, P. Schmölz, W. S. M. Werner, and H. Störi, *in* "High Tech in Salzburg—Creativity in Advanced Materials and Process Engineering" (R. W. Lang and M. A. Erath, Eds.), p. 141. SAMPE, Niederglatt, 1995.
60. C. Mitterer, H.-M. Ott, J. Komenda-Stallmaier, P. Schmölz, W. S. M. Werner, and H. Störi, *J. Alloys Compounds,* **239**(2), 183 (1996).
61. V.-H. Derflinger, W. Waldhauser, C. Mitterer, P. Schmölz, and H. Störi, *Thin Solid Films* **286,** 188 (1996).
62. T. Shikama, Y. Sakai, M. Fukutomi, and M. Okada, *Thin Solid Films* **156,** 287 (1988).
63. G. Sade and J. Pelleg, *Appl. Surf. Sci.* **91,** 263 (1995).
64. I. Petrov, I. Ivanov, V. Orlinov, and J.-E. Sundgren, *J. Vac. Sci. Technol. A* **5,** 2733 (1993).
65. J. E. Greene, *in* "Handbook of Crystal Growth" (D. T. J. Hurle, Ed.), Vol. 1, p. 640. Elsevier, Amsterdam, 1993.
66. G. Betz, M. Opitz, and P. Braun, *Nucl. Instrum. Methods* **182–183,** 63 (1981).
67. J. A. Thornton, *in* "Deposition Technologies for Films and Coatings" (R. F. Bunshah, Ed.), p. 170. Noyes, Park Ridge, NJ, 1982.
68. M. Konuma, "Film Deposition by Plasma Techniques." Springer-Verlag, Berlin, 1992.
69. I. Petrov, I. Ivanov, V. Orlinov, and J.-E. Sundgren, *J. Vac. Sci. Technol. A* **5,** 2733 (1993).
70. A. J. Perry, *Thin Solid Films* **138,** 73 (1986).
71. K. Ploog, H. Schmidt, E. Amberger, G. Will, and K. H. Kossobutzki, *J. Less-Common Met.* **29,** 161 (1972).
72. C. Mitterer, P. Rödhammer, H. Störi, and F. Jeglitsch, *J. Vac. Sci. Technol. A* **4,** 2646 (1989).
73. P. Rogl and P. E. Potter, *CALPHAD* **2,** 191 (1988).
74. Powder Diffraction File, Joint Committe on Powder Diffraction Standards, International Center for Diffraction Data, Swarthmore, PA, Cards 35-741, 34-432, 6-0401, 11-670, 24-1120.
75. J.-E. Sundgren, *Thin Solid Films* **128,** 21 (1985).
76. R. Kieffer and F. Benesovsky, "Hartstoffe," p. 382–392. Springer-Verlag, Wien, 1963.
77. P. B. Barna, *in* "Diagnostics and Applications of Thin Films" (L. Eckertová and T. Ruzicka, Eds.), p. 295. Institute of Physics, Bristol, 1992.
78. F. Vollertsen and C. Mitterer, *in* 'Reibung und Verschleiß" (H. Grewe, Ed.), p. 107. DGM Informationsgesellschaft, Oberursel, 1992.
79. J. Aromaa, H. Ronkainen, A. Mahiout, S.-P. Hannula, A. Leyland, A. Matthews, B. Matthews, and E. Broszeit, *Mater. Sci. Eng. A* **140,** 722 (1991).
80. M. Ürgen, A. F. Çakir, O. L. Eryilmaz, and C. Mitterer, *Prakt. Metallographie* **3,** 126 (1995).
81. C. Mitterer, O. Heuzè, and V.-H. Derflinger, *Surf. Coat. Technol.* **89,** 233 (1997).
82. B. Elsener, A. Rota, and H. Böhni, *Mater. Sci. Forum* **44/45,** 28 (1989).
83. M. Ürgen, A. F. Çakir, O. L. Eryilmaz, and C. Mitterer, "Interfinish 96," 10–12, September 1996, Birmingham, in press.
84. F. W. Billmeyer, *Color Res. Appl.* **3,** 140 (1988).
85. U. Beck, G. Reiners, I. Urban, and K. Witt, *Thin Solid Films* **220,** 234 (1992).
86. E. Kierzek-Pecold, *Phys. Stat. Sol.* **33,** 523 (1969).
87. V. I. Bessaraba, L. A. Ivanchenko, and Yu. B. Paderno, *J. Less-Common Met.* **67,** 505 (1979).
88. A. I. Shelykh, K. K. Sidorin, M. G. Karin, V. N. Bobrikov, M. M. Kursukova, V. N. Gurin, and I. A. Smirnov, *J. Less-Common Met.* **82,** 291 (1981).
89. P. A. M. van der Heide, H. W. ten Cate, L. M. ten Dam, R. A. de Groot, and A. R. de Vroomen, *J. Phys. F: Metal Phys.* **16,** 1617 (1986).
90. R. E. Hummel, "Electronic Properties of Materials," Springer-Verlag, Berlin, 1993.
91. J. M. Lafferty, *J. Appl. Phys.* **22,** 299 (1951).